Bending and Circularization of Site-Specific and Stereoisomeric Carcinogen−DNA Adducts†

Rong Xu,‡,§ Bing Mao,‡,⊥ Shantu Amin,|| and Nicholas E. Geacintov*,‡

Chemistry Department, MC 5180, New York University, New York, New York 10003, and American Health Foundation, Valhalla, New York 10595

Received July 22, 1997; Revised Manuscript Received November 5, 1997⊗

ABSTRACT: The potent tumorigen and mutagen (+)-7(*R*),8(*S*)-dihydroxy-9(*S*),10(*R*)-epoxy-7,8,9,10-tetrahydrobenzo[*a*]pyrene ((+)-*anti*-BPDE) is a metabolite of benzo[*a*]pyrene that binds predominantly to the exocyclic amino group of guanine residues in DNA *in vivo* and *in vitro*. While the (−)-7*S*,8*R*,9*R*,10*S* enantiomer, (−)-*anti*-BPDE, also reacts with DNA to form similar covalent N^2-deoxyguanosyl adducts, this diol epoxide is nontumorigenic and its mutagenic activities are different from those of (+)-*anti*-BPDE. In this work, T4 ligase-induced cyclization methods have been employed to demonstrate that the (+)-*anti*-[BP]-N^2-dG lesions (G*) cause significantly greater amounts of bending and circularization of the one-base overhang undecamer duplex 5′-d(CACAT[G*]TACAC)·d(TGTACATGTGG) than the stereoisomeric oligonucleotide duplex with G* = (−)-*anti*-[BP]-N^2-dG. In the case of the (+)-*anti*-BPDE-modified oligonucleotides, the ratio of circular to linear DNA multimers reaches values of 8−9 for circle contour sizes of 99−121 base pairs, while for the (−)-*anti*-[BP]-N^2-dG-modified DNA this ratio reaches a maximum value of only ∼1 at 154−176 base pairs. Assuming a planar circle DNA model, the inferred bending angles for 90−92% of the observed circular ligation products range from 30 to 51° per (+)-*trans*-*anti*-[BP]-N^2-dG lesion and from 20 to 40° per (−)-*trans*-*anti*-[BP]-N^2-dG lesion. In the case of unmodified DNA, the probability of circular product formation is at least 1 order of magnitude less efficient than in the BPDE-modified sequences and about 90% of the circular products exhibit bending angles in the range of 14 −19°. In the most abundant circular products observed experimentally, the bending angles are 40° and 26 ± 2° per (+)-*anti*-[BP]- or (−)-*anti*-[BP]-modified 11-mer; these values correspond to a net contribution of 21−26° and 5−19°, respectively, to the observed overall bending per lesion. The coexistence of circular DNA molecules of different sizes and, therefore, different average bending angles per lesion, suggest that the lesions induce both torsional flexibility and flexible bends, which permit efficient cyclization, especially in the case of (+)-*trans*-[BP]-N^2-dG adducts. The NMR characteristics of (+)-*trans*-[BP]-N^2-dG lesion in the 11-mer duplex 5′-d(CACATG*]TACAC)·d(GTGTACATGTG) indicate that all base pairs are intact, except at the underlined base pairs. This suggests a distortion in the normal conformation of the duplex on the 5′-side of the modified guanosine residue, which may be due to bending enhanced base pair opening and bending induced by the bulky carcinogen residue. The implications of base sequence-dependent flexibilities and conformational mobilities of *anti*-[BP]-N^2-dG lesions on DNA replication and mutation are discussed.

Benzo[*a*]pyrene is a pervasive environmental pollutant that is metabolized in living cells to a number of highly reactive and electrophilic derivatives (*1*). The diol epoxides (+)-7(*R*),8(*S*)-dihydroxy-9(*S*),10(*R*)-epoxy-7,8,9,10-tetrahydrobenzo[*a*]pyrene and the enantiomer (−)-7(*S*),8(*R*)-dihydroxy-9(*R*),10(*S*)-epoxy-7,8,9,10-tetrahydrobenzo[*a*]pyrene, [(+)-*anti*-BPDE and (−)-*anti*-BPDE,[1] respectively], are of particular interest for structure−activity correlation studies. The (+)-enantiomer is highly tumorigenic, while its mirror-image isomer (−)-*anti*-BPDE is inactive in rodents (*2*, *3*). The mutagenic activities of this pair of enantiomers are also significantly different both in mammalian and in bacterial cells (*4*−*7*). Both *anti*-BPDE enantiomers are known to react with native DNA by forming covalent adducts mainly by *trans*-addition of the exocyclic amino group of guanine to the C10 position of *anti*-BPDE (*8*, *9*); the structures of these two stereoisomeric *trans*-*anti*-[BP]-N^2-dG adducts are com-

† This research was supported by a grant from the Office of Health and Environmental Research, Department of Energy (DE-FGO2-86ER60405), and in part by the NIH, National Cancer Institute (Grant No. CA 20851). The benzo[*a*]pyrene diol epoxides were supplied by the National Cancer Institute Carcinogen Reference Standard Repository.

‡ New York University.

§ Rockefeller University, Box No. 163, New York, NY 10021.

|| American Health Foundation.

⊥ Present Address: Cellular Biochemistry and Biophysics Program, Memorial Sloan-Kettering Cancer Center, New York, NY 10021.

⊗ Abstract published in *Advance ACS Abstracts,* December 15, 1997.

[1] Abbreviations: (+)-*anti*-BPDE, (+)-7(*R*),8(*S*)-dihydroxy-9(*S*),10(*R*)-epoxy-7,8,9,10-tetrahydrobenzo[*a*]pyrene; (−)-*anti*-BPDE, (−)-7(*S*),8(*R*)-dihydroxy-9(*R*),10(*S*)-epoxy-7,8,9,10-tetrahydrobenzo[*a*]pyrene; (+)- or (−)-*trans*-[BP]-N^2-dG: 2′-deoxyguanosyl adduct derived from the *trans*-addition of the exocyclic amino group to the C10 position of (+)- or (−)-*anti*-BPDE.

S0006-2960(97)01785-6 CCC: $15.00
Published on Web 01/13/1998

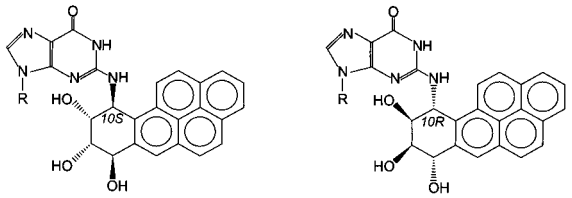

FIGURE 1: Structures of the 10*S* (+)- and 10*R* (−)-*trans*-[BP]-N^2-dG adducts incorporated in the duplex sequence **I**.

pared in Figure 1.

The relationships between the biological impact and the conformations of these and related adducts are subjects of great current interest [reviewed in ref *10*]. The three-dimensional conformations in aqueous solutions of the (+)- and (−)-*trans*-[BP]-N^2-dG lesions have been investigated by high resolution NMR techniques (*11*−*13*); in both cases, the aromatic pyrenyl residues are positioned in the minor groove of B-form DNA pointing into the 5′-direction in the case of the 10*S* (+)-*trans*- and into the 3′-direction of the modified strand in the case of the 10*R* (−)-*trans*-adduct. These striking opposite orientations of the polynuclear aromatic residues relative to the modified base influence the rates of digestion of oligonucleotides by exonucleases (*14*), the *in vitro* efficiencies of UvrABC-mediated nucleotide excision repair (*15*), transcription (*16*), and DNA replication *in vitro* (*17*, *18*) and in bacterial and mammalian cells (*19*−*21*).

Alterations in the three-dimensional shapes or dynamic characteristics of carcinogen-modified DNA sequences due to adduct-induced bends and flexible hinge joints (*22*, *23*) may also influence the cellular processing of these lesions. Gel electrophoresis (*24*) and flow linear dichroism experiments (*25*−*27*) with *anti*-BPDE-modified native DNA and synthetic polynucleotides have shown that covalent BPDE−DNA lesions induce bends or increase the flexibility of DNA. However, because the DNA was randomly modified, the distribution of adducts was heterogeneous (*8*, *9*); thus, the relationships between the stereochemical characteristics and the effects of base sequence context on bending could not be established. These uncertainties can be overcome by working with site-specific and stereochemically defined oligodeoxynucleotide adducts. Using this approach, it has been shown more recently that DNA bending associated with *anti*-[BP]-N^2-dG lesions is dependent not only on the stereochemical characteristics of these lesions (*28*, *29*) but also on the bases flanking these lesions (*30*).

The curvature and flexibility of carcinogen-modified DNA can be conveniently studied by making use of the anomalously slow migration of bent DNA duplexes in polyacrylamide gels (*31*−*33*). Indeed, the bending of DNA induced by covalently bound chemicals has been successfully analyzed by gel electrophoresis methods (*22*, *23*, *34*−*36*). The degree of intrinsic bending can be analyzed either by ligase-induced direct cyclization methods (*37*, *38*) or by comparing the electrophoretic mobilities of modified and unmodified linear DNA multimers (see, for example, ref *39*).

In this work, we have employed the direct cyclization method to compare the flexibilities and the extent of bending induced by the stereoisomeric (+)-*trans*-[BP]-N^2-dG and (−)-*trans*-[BP]-N^2-dG lesions (G*) in the 11-mer oligonucleotide duplexes:

3′-d(GGTGTA-C--ATGT)
5′-d(CACAT[G*]TACAC) **(I)**

This sequence was selected because the effects of thymidine residues flanking the *anti*-[BP]-N^2-dG lesions (5′-...TG*T... sequence context) are believed to enhance the local flexibility, permitting the interconversion between two or more adduct conformers (*10*, *13*). In contrast, when *anti*-BPDE-modified dG residues are flanked by cytidine residues (5′-...CG*C...), only one adduct conformation was observed (*11*) and the bend associated with the adduct is rigid rather then flexible.[2] The one-base overhangs in sequence **I** at each end of the duplexes serve to form noncovalent complexes that can be covalently sealed by T4 ligase to form linear and circular multimers of different sizes. Oligonucleotide 11-mer duplexes **I** containing the stereoisomeric (+)- or (−)-*cis*-[BP]-N^2-dG lesions are more difficult to ligate (*28*). Therefore, only the *trans* adducts derived from (+)- and (−)-*anti*-BPDE were selected for further quantitative analysis of BPDE-induced bending in sequence **I**. Since runs of CA sequences are known to be flexible (*40*), the unmodified sequence **I** was also self-ligated and the products served as a reference for the results obtained with the BPDE-modified sequences.

MATERIALS AND METHODS

The undecamers d(CACATGTACAC), d(TGTACATGTGG), and d(GTGTACATGTG) were synthesized using a Biosearch Cyclone DNA synthesizer and were purified by standard HPLC protocols (*41*). The method of synthesis and the characteristics of the site-specific BPDE-modified oligonucleotide adducts in the sequence d(CACATGTACAC) have already been described (*42*, *43*).

Forward reaction 5′-end labeling of both unmodified and modified oligonucleotides with [γ-^{32}P]ATP (New England Nuclear) and cold ATP (Pharmacia) was employed as described previously (*28*). The complementary oligonucleotides were cold-labeled at the 5′-end. The labeled oligonucleotides were separated from the unlabeled ones by denaturing electrophoresis in 20% polyacrylamide gels. A 100-base pair DNA ladder (Gibco BRL), used as a size marker, was 5′-end labeled by T4 polynucleotide kinase in a phosphate exchange reaction. All samples were desalted using chromatography cartridges (Biorad).

The complementary strands d(TGTACATGTGG) were added in 2.5-fold excess to the unmodified and modified d(CACATGTACAC) strands in order to ensure that the oligonucleotides would be in the duplex form during the ligation reaction (*28*). The ligation reaction was conducted with 1 unit of T4 ligase (Gibco BRL) added for every 5 pmol of double-stranded DNA, with the duplex undecamer concentration at 4 μM, or 20 μM, in 1x ligation buffer (Gibco BRL). The ligated DNA multimer mixtures were subjected to one-dimensional (1-D) and two-dimensional (2-D) nondenaturing (29:1 acrylamide to bisacrylamide) gel electrophoresis at 4 °C. In 2-D gel electrophoresis, gel concentrations varied from 6 to 12% for the first dimension and from 7 to 12% for the second dimension in the presence of

[2] Hong Tsao, Bing Mao, Rong Xu, Shantu Amin, and Nicholas E. Geacintov (submitted for publication).

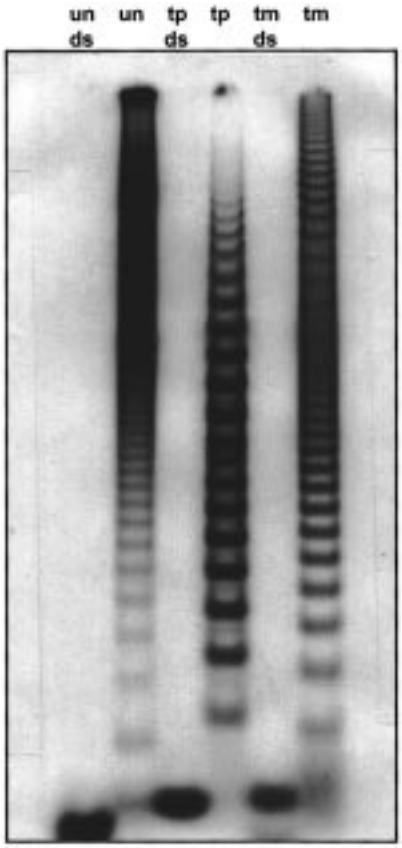

FIGURE 2: Autoradiograph of a nondenaturing gel in 6% polyacrylamide (29:1 acrylamide:bis-acrylamide). Lane: un ds, unligated and unmodified duplex **I**; tp ds, unligated (+)-oligonucleotide duplex **I** (G* = (+)-*trans*-[BP]-N^2-dG); tm ds, unligated (−)-oligonucleotide duplex **I** (G* = (−)-*trans*-[BP]-N^2-dG). Lane: un, mixture of ligated unmodified oligonucleotide duplex **I**; tp, mixture of ligated (+)-*trans*-oligonucleotide duplex **I**; tm, mixture of ligated (−)-*trans*-oligonucleotide duplex **I**. The initial undecamer concentrations were 20 μM in all cases.

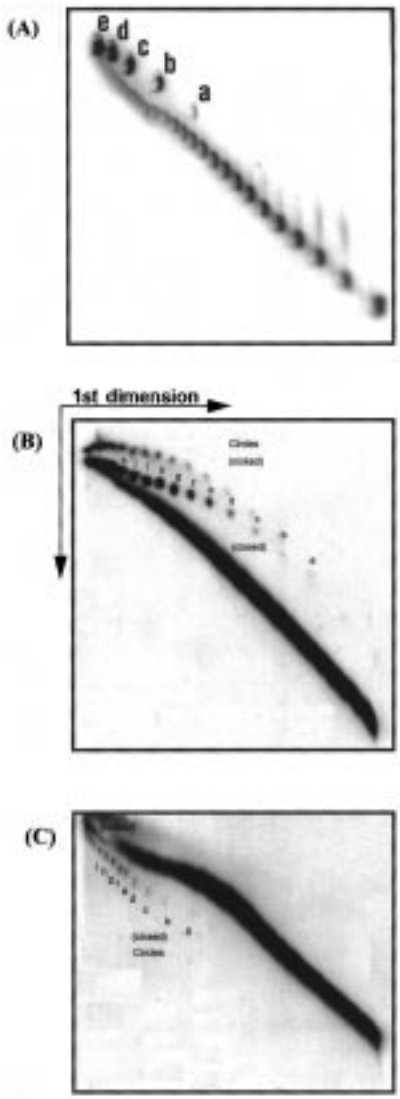

FIGURE 3: (A) Two-dimensional gel electrophoresis of the ligation mixture of (+)-*trans*-oligonucleotide duplex **I**. First dimension (horizontal): 12% polyacrylamide gel. Second dimension: 12% polyacrylamide gel containing 50 μg/mL chloroquine. Spots labeled a−e are cyclic ligation products. (B) Two-dimensional gel electrophoresis of the ligation mixture of (−)-*trans*-oligonucleotide duplex **I**. First dimension (horizontal): 6% polyacrylamide gel. Second dimension: 8% polyacrylamide gel containing 50 μg/mL chloroquine. Spots labeled a−k are cyclic ligation reaction products. (C) Two-dimensional gel electrophoresis of the ligation mixture of unmodified oligonucleotide duplex **I**. First dimension (horizontal): 6% polyacrylamide gel. Second dimension: 7% polyacrylamide gel containing 50 μg/mL chloroquine. Spots labeled a−i are cyclic ligation reaction products.

chloroquine (1 μg/mL), in both the gel and buffer solutions (*38*). The sizes of the circles formed upon ligation in the mixtures were evaluated using multiple-step procedures. First, the DNA mini-circles were isolated from the gels after 2-D nondenaturing gel electrophoresis and were eluted with 0.5 M ammonium acetate−0.01 M magnesium diacetate buffer overnight at 25 °C. The salt was removed by two successive ethanol precipitations. The circular DNA was then redissolved in 4 μL of 90% (wt/vol) formamide in 0.1 M Tris−HCl buffer (pH = 7.4) and heated at 100 °C for 10−15 min in order to introduce nicks into the circular DNA molecules. The samples were then subjected to electrophoresis in 8% denaturing polyacrylamide gels (19:1 acrylamide:bisacrylamide, 7 M urea). The gels were subjected to quantitative analysis using a BIORAD 250 imaging system (Biorad).

RESULTS

Ligation Ladders: Formation of Circularized DNA Molecules. Typical gel electrophoresis patterns of ligation mixtures of unmodified duplexes **I** (un) and of duplexes **I** with (+)-*trans* and (−)-*trans*-[BP]-N^2-dG lesions (labeled tp and tm, respectively) are shown in Figure 2. The unligated double-stranded 11-mers (labeled ds) define the positions of the shortest duplexes in the ligation mixtures. The relative mobilities are highest for the ligated unmodified sequences and smallest in the case of the (+)-*trans*-adduct-containing samples, as discussed earlier (*28*).

Evidence for the formation of cyclic DNA was sought using 2-D nondenaturing gel electrophoresis methods (*38*). The 2-D gel autoradiographs of ligation products of BPDE-modified and unmodified oligonucleotides are shown in Figure 3A−C. The upper sets of spots in Figures 3A and 3B and the set of lower spots in Figure 3C are attributed to circular DNA molecules (*38, 44*). In Figure 3A, the bands due to the individual linear multimers are positioned on an approximately diagonal line and can be clearly distinguished. In Figures 3B and 3C, the individual bands are not resolved

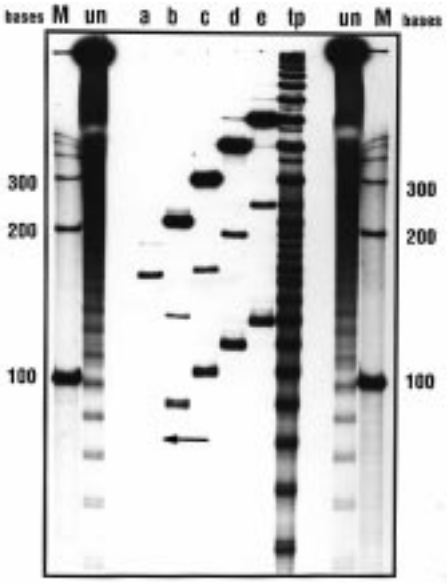

FIGURE 4: Denaturing gel electrophoresis in 8% polyacrylamide for estimating the sizes of the circular DNA products with (+)-*trans*-[BP]-N^2-dG lesions. Lanes M: 100-base interval size markers. Lanes un: ligation mixture of unmodified duplex **I** with the individual bands serving as size markers. Lanes a−e: cyclic DNA products isolated from the gel shown in Figure 3A, after treatment with a hot formamide solution. Lane tp: crude ligation mixture of (+)-*trans*-oligonucleotide duplex **I** after treatment with a hot formamide solution. The arrow indicates the position of a faint band in lane a that was visible in the original gel.

from one another because it was necessary to overexpose the films in order to visualize the less abundant circular DNA bands. The bands labeled a−e in Figure 3A and a−k in Figure 3B are due to covalently closed circular DNA molecules, whereas the upper, more slowly migrating bands in Figure 3B are identified as nicked circular DNA molecules (*38*, *44*). In Figure 3C, depicting the 2-D migration patterns of unmodified ligated sequences **I**, the circular multimers appear to migrate faster in the second dimension than the linear multimers; the faster mobilities of the unmodified circular DNA molecules relative to the linear ones in Figure 3C may be associated with a greater extent of overwinding of the circular DNA induced by the intercalator chloroquine. Further studies of this effect were beyond the scope of this work.

Analysis of Circle Sizes. The extent of bending can be estimated from an analysis of the number of base pairs per molecule in the circular DNA molecules. The contents of the circular DNA bands (Figure 3) were excised and treated with a hot formamide solution. Using denaturing 8% polyacrylamide gels, the sizes of the resulting cleaved single strands were compared to those of the linear molecules produced by ligation of the 11-mer oligonucleotide adducts as previously described (*38*, *44*).

The gel patterns of the circular DNA derived from the ligation of (+)-*trans*-[BP]-modified oligonucleotides are shown in Figure 4. The relative mobilities of markers 100, 200, 300, etc. bases long are shown in lanes M. The lanes un represent the mobility patterns of ligation products of the unmodified undecamer, showing bands that are 55, 66, 77, 88, 99, etc. bases long, corresponding to $n = 5$, 6, 7, 8, and 9 ligated monomer units, respectively. Lanes a−e, represent the mobility patterns of the hot formamide-treated circular DNA molecules extracted individually from the similarly labeled spots in the gel depicted in Figure 3A. In these lanes, the fastest migrating band represents the linearized, ^{32}P-5′-end-labeled DNA molecules, the intermediate mobility band represents the single-stranded covalently closed circular DNA molecule, while the slowest band represents the double-stranded covalently closed circular DNA (*38*).

Lane tp represents the electrophoresis pattern of all of the ligation products of (+)-*trans*-[BP]-modified oligonucleotide duplexes I treated with hot formamide. The lengths of these tp bands can be determined from a comparison of their positions relative to those in the adjacent un lane; because of the presence of the BPDE residue, the [BP]-modified single-stranded sequences in lane tp migrate somewhat slower than the unmodified strands in lane un. Starting from the bottom, the lower five bands in lane tp are identified as multimers 55, 66, 77, 88, and 99 bases long (bottom to top). If we now compare the migration distances of the lowest bands in lanes a−e with those in the tp lane in Figure 4, the lowest bands due to the linear fragments line up with adjacent bands of different sequence lengths in the tp lane; the lowest band in lane a is very faint and its position in this gel photograph is indicated by the horizontal arrow. From these comparisons, the sizes of the linearized bands in lanes a−e and, therefore, the sizes of the circular DNA molecules in bands a−e in Figure 3A, can be established. These differ successively from one another in size by 11 base pairs, and their contour lengths are 77, 88, 99, 110, and 121 base pairs, respectively. Thus, the circular DNA spots a−e in Figure 3A result from the ligation of 7, 8, 9, 10, and 11 undecamers **I**.

Similar analyses of the sizes of the circular DNA molecules formed from the ligation of (−)-*trans*-oligonucleotide 11-mer duplexes **I** are shown in Figure 5. The lanes c−j represent the migration patterns of the identically labeled circular DNA spots in the native, nondenaturing 2-D gels in Figure 3B. The lowest bands in lanes e−j line up with those due to the 13-mer, 14-mer, 15-mer, 16-mer, 17-mer, and 18-mer bands in lane tm. The sizes of these circular DNA molecules in the native 2-D gels in Figure 5 are therefore 143−191 bases pairs. The lowest bands in lanes c and d are not visible, although the top bands (covalently closed circular molecules) are prominent at the top of the gel. Thus, spots c and d in Figure 3B most likely represent circular DNA molecules 121 and 132 base pairs in size, respectively. The spots a and b in the 2-D gel in Figure 3B were too faint to be analyzed but are discernable in the phosphorimager traces (data not shown); these spots most likely represent circular DNA molecules 99 and 110 base pairs in size.

The results obtained with the unmodified oligonucleotide duplexes **I** are shown in Figure 6. The fraction of circular DNA molecules is significantly lower than in the ligated (+)-*trans*- and (−)-*trans*-oligonucleotide duplexes **I**, and there were insufficient amounts of circular DNA in spots a−c in Figure 3C for analysis by the denaturing gel method. The bands due to the linear, highest mobility bands in lanes d−i are also quite faint, and their positions in lanes d−e are indicated by the horizontal arrows in Figure 6. The lowest bands, due to the linearized DNA molecules, in lanes d−i line up with the bands in lane cntl that are due to the ligated linear DNA molecules 220−275 bases long. The corresponding circularized DNA molecules (spots d−i in Figure

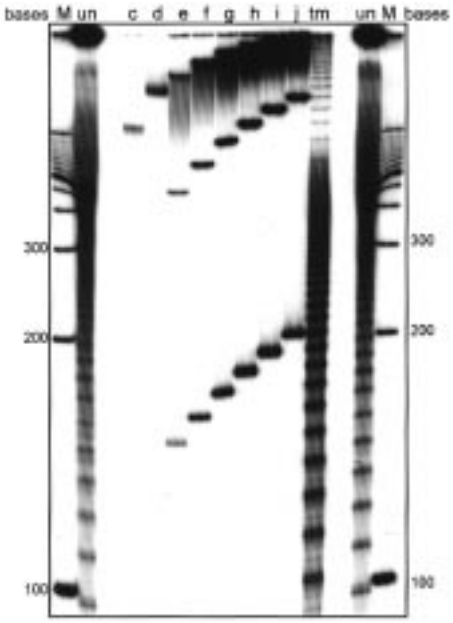

FIGURE 5: Denaturing gel electrophoresis in 8% polyacrylamide for estimating the sizes of the circular DNA products with (−)-*anti*-[BP]-N^2-dG lesions. Lanes M: 100-base interval size markers. Lanes un: ligation mixture of unmodified duplex **I** with the individual bands serving as size markers. Lanes c−j: cyclic DNA products isolated from the gel shown in Figure 3B, after treatment with a hot formamide solution. Lane tm: crude ligation mixture of (−)-*trans*-oligonucleotide duplex **I** after treatment with a hot formamide solution.

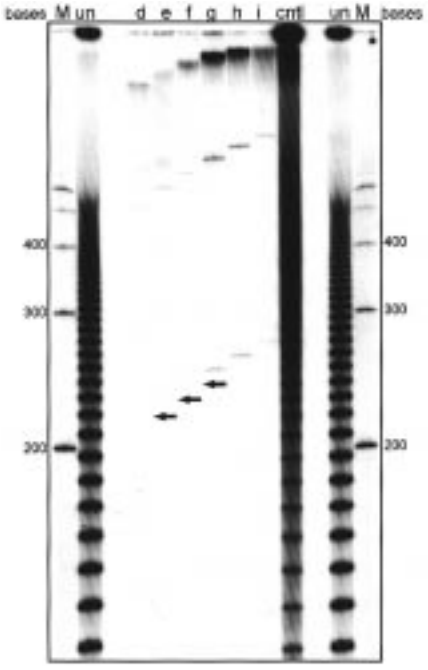

FIGURE 6: Denaturing gel electrophoresis in 8% polyacrylamide for estimating the sizes of the circular unmodified DNA products. Lanes M: 100-base interval size markers. Lanes un: ligation mixture of unmodified duplex I with the individual bands serving as size markers. Lanes d−i: cyclic DNA products isolated from the gel shown in Figure 3C, after treatment with a hot formamide solution. Lane cntl: crude ligation mixture of (−)-*trans*-oligonucleotide duplex **I** after treatment with a hot formamide solution. The arrows indicate the positions of faint bands in lanes d−f, that were more clearly visible in the original gel.

6) are thus 20−25 unmodified undecamers, or 220−275 base pairs in size. The circular DNA bands a, b, and c (the band a is too faint to be visible in the photograph of the gel shown in Figure 3C) are attributed to circles 187, 198, and 209 base pairs in size.

Circularization Efficiencies. The relative distributions of circular and linear ligation products were studied at two different starting undecamer duplex concentrations (4 and 20 μM) since the product ratio can depend on the starting DNA concentration (*44*, *45*). The reactions were carried out to the endpoint, defined as the loss of activity of the enzyme, which occurs after a reaction time of about 15 h.

The fractions of circular and linear DNA fragments (Figure 7) were determined from an analysis of the 1-D phosphorimager density profiles of the ligation products by integration of the areas under each linear and each circular DNA band. These values were divided by the number of ligated 11-mers per molecule in order to compensate for the length-dependent increase in the radioactivities of the ligation products.

(+)-trans-[BP]-Modified Oligonucleotides. At the 4 μM initial duplex concentration, linear multimers dominate below 77 base pairs ($n < 7$). However, for $n = 8$, the ratio of circular to linear ligation products, N_{circ}/N_{lin}, is 2.3 and rises to a maximum value of 7.9 at $n = 10$, corresponding to 110 base pairs, before dropping off to a value of 2.8 at $n = 13$ (Figure 7A). At the higher, 20 μM starting concentration, there is a decrease in the fractions of the lower molecular weight fragments and a shift in the distribution of the linear multimers from the smaller towards the larger sizes (Figure 7A′). The ratio of circular to linear products reaches a maximum of 8.6 at $n = 12$.

(−)-trans-[BP]-Oligonucleotides. The ratios of circular to linear ligation products is ∼1, or less (Figure 7B,B′). Cyclization is considerably less efficient than in the case of the (+)-*trans*-[BP]-modified oligonucleotide duplexes, and the maxima in the ratios of circular to linear products shift toward $n = 14$ and 15−16 at the 4 and 20 μM initial DNA concentrations, respectively. The size distributions are broader than in the (+)-*trans*-adduct case at both DNA concentrations, but the sizes of the smallest circular DNA molecules are similar in these ligated stereoisomeric *trans*-oligonucleotide duplexes. The relative amounts of circular to linear products decrease for all multimer sizes at the higher starting DNA concentration, as expected when circularization is relatively inefficient (*44*).

Unmodified Oligonucleotides. In the case of the unmodified 11-mer oligonucleotide duplexes **I**, the overall cyclization efficiency is lower than in both of the BPDE-modified 11−mers at the 4 μM concentration (Figure 7C). The overall fraction of circular products decreases by a factor of ∼3 when the DNA concentration is increased from 4 to 20 μM (Figure 7C′). At the 20 μM DNA concentration, there is a shift in the distribution toward larger molecular weight linear forms. The smallest observable circles are 187−198 base pairs in size ($n = 17$−18), and a plateau in the distribution is reached in the range of ∼231−286 base pairs (Figure 7C,C′). These observations are similar to those reported for the ligation and circular multimer formation of other unmodified DNA sequences (*37*, *46*); the formation of circular products is believed to reflect the natural thermal flexibilities of the DNA molecules (*40*).

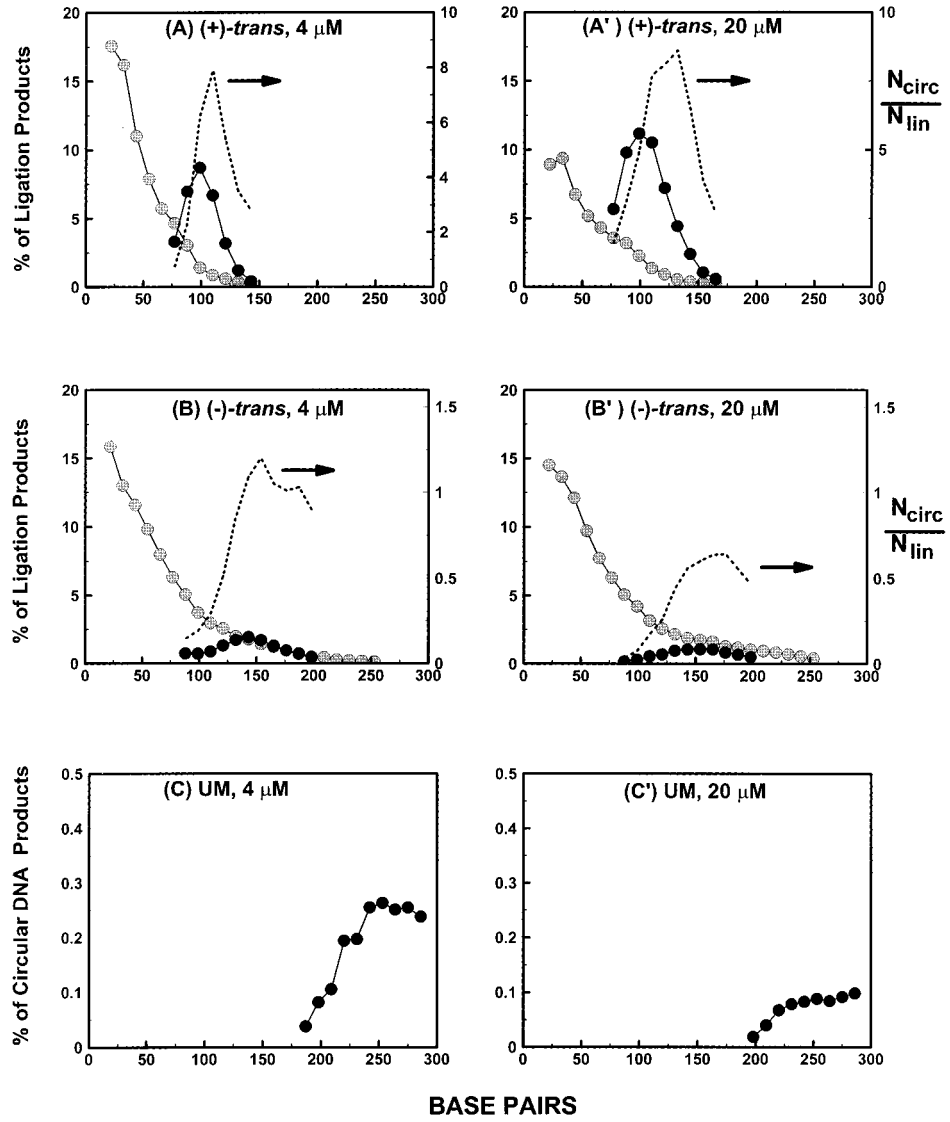

FIGURE 7: Relative efficiencies (percentage of total products) of formation of linear (gray circles) and circular (black circles) products resulting from the ligation of oligonucleotide duplexes **I** as a function of size (expressed in number of base pairs) of the linear or circular multimers. The dotted lines represent the ratios of circular to linear multimers (N_{circ}/N_{lin}) as a function of size (the arrows indicate that the scale for the dotted curves are on the right-hand abscissa). Starting 11-mer duplex **I** concentrations in the ligation mixtures were 4 μM (panels A−C) and 20 μM (panels A′−C′). Key: A, A′, (+)-*trans*-[BP]-modified oligonucleotide duplex I; B, B′, (−)-*trans*-[BP]-modified oligonucleotide duplex I; C, C′, unmodified oligonucleotide duplex I. In the case of the unmodified DNA (panels C and C′), the relative abundance of circular DNA molecules is rather low; thus, longer film exposures were needed in order to visualize these bands. Under these conditions, the individual bands due to the linear molecules overlap and could no longer be resolved.

DISCUSSION

General considerations suggest that the formation of circular DNA molecules should be unfavorable for short DNA fragments because the extent of bending may be insufficient for the two ends to meet. On the other hand, the probability of the two ends of the same molecule coming together tends to diminish as the length of the fragments increases (*37*, *47*, *48*). These considerations account for the maxima in the distributions of circular ligation products in Figure 7. The (+)-*trans-anti*-[BP]-N^2-dG moieties and, to a lesser extent the (−)-*trans*-lesions, centrally incorporated into oligonucleotide duplexes **I**, greatly enhance the probabilities of circularization (Figure 7). Since cyclization competes with the condensation of oligonucleotides to form linear molecules, an increase in the starting DNA concentration might increase the efficiency of formation of linear condensation products (*37*, *45*, *49*). Indeed, as the starting DNA concentration is increased from 4 to 20 μM, the proportions of circular products decrease from 13% to 8% in the case of the (−)-*trans*-[BP]-modified oligonucleotide duplexes **I** (Figure 7B,B′). However, in the case of the (+)-*trans*-[BP]-modified oligonucleotides, a similar increase in the DNA concentration increases the fraction of circular DNA molecules from about 50% at the 4 μM to about 70% at the 20 μM initial DNA concentration; this increase occurs primarily at the expense of low molecular weight linear DNA fragments and is a manifestation of the extraordinary efficiency of circularization of oligonucleotides with (+)-*trans-anti*-[BP]-N^2-dG lesions (Figure 7A,A′). Further interpretations of these DNA concentration effects would have required detailed kinetic studies (*37*, *45*, *48*) that were beyond the scope of this work.

Average Bending Angles. The bending angles associated with the covalently bound BP residues can be estimated,

assuming that the circular DNA molecules are planar, by dividing 360° by the number of monomeric undecamer units per circle (*44*, *50*).

In the case of (+)-*trans*-[BP]-modified oligonucleotides, the most abundant circular DNA molecules consists of 99 base pairs or nine undecamer units with bending angles of ~40°. The smallest and largest observed circular DNA molecules contain 77 and 165 base pairs at the extremes of the distribution. However, 92% of the circular products exhibit sizes within the 77−121 base pair range, thus encompassing a range of bending angles of 30−51°.

In the case of (−)-*trans*-[BP]-modified oligonucleotides, the maximum in the circle size distribution occurs at *n* values of 11−15 (Figure 7B,B′) with bending angles in the range of 24−33°. The smallest and largest observed circle sizes are 8 and 18 undecamers in size, respectively, with 90% of the circles falling within the 99−188 base pair range, corresponding to bending angles per adduct of 20−40°.

A variety of unmodified DNA sequences exhibit curvature and flexibility, thus contributing to circular DNA formation upon ligation (*40*, *51*, *52*). The unmodified undecamer sequence **I** is no exception. A maximum in the distribution of circle sizes occurs near ~242 base pairs (Figure 7C,C′) and 92% of the observed circular ligation products are 209−286 base pairs in size, corresponding to bending angles of 14−19° per undecamer. These values correspond to bending angles of ~1.3−1.7° per base pair; these values are close to the average value of 1.3° per base pair associated with native viral DNA sequences (*37*). The natural bending of the unmodified sequence of 14−19° per undecamer duplex **I** is significantly smaller than the bending angles of ~30−51° associated with the 11-mer duplexes containing the (+)-*trans*-*anti*-[BP]-N^2-dG lesion. The bending associated with the (−)-*trans*-*anti*-[BP]-N^2-dG lesions (20−40°) tends to be smaller than in the case of the (+)-*trans*-*anti*-[BP]-N^2-dG adducts but is larger than in the case of the unmodified sequence.

The ranges of observed circular DNA sizes suggest that the BPDE-modified and unmodified sequences can assume a range of bending angles probably due to an inherent or BPDE adduct-enhanced flexibility. The net contributions of the BPDE-modified GC base pairs in duplex **I** to the overall bending can be estimated by subtracting the effects associated with the natural flexibility or bending of 14−19° per unmodified 11-mer from the most probable bending angles of 40° ((+)-[BP]-N^2-dG lesion) and 24−33° ((−)-[BP]-N^2-dG lesion); the net contributions per modified dG-dC base pair is thus 21−26° and 5−19°, respectively.

Bending, Flexibility, and Cyclization Efficiency. While the range of observed bending angles in the (+)-*trans*- and (−)-*trans*-[BP]-modified oligonucleotide adducts are comparable, the cyclization of the (+)-*trans*-adducts is strikingly more efficient. The extraordinarily high cyclization efficiencies for DNA fragments 99 ± 22 base pairs long with (+)-*trans*-[BP]-N^2-dG lesions (Figure 7A,A′) in the ...TG*T... sequence context of duplex **I**, as well as the range of circle sizes and observed bending angles of 30−51°, suggest that the bends arise from a flexibility at the sites of the lesions, rather than from a set of conformers, each associated with a different static bending angle. This conclusion is supported by recent results that show that the gel electrophoretic mobilities of ligated multimers **I** with the same same base sequences flanking the (+)-*trans*-[BP]-N^2-dG lesions are independent of the phasing between the lesions and the helical repeat.[2]

In the case of the (−)-*trans*-[BP]-N^2-dG lesions, the range of inferred bending angles (20−40°) is not markedly different from that of the (+)-*trans*-[BP]-N^2-dG lesions, but the probability of cyclization is nearly 1 order of magnitude smaller. We conclude that the flexibility associated with the *trans*-adducts derived from the (−)-*anti*-BPDE enantiomer is thus significantly smaller than the flexibility associated with (+)-*trans*-*anti*-[BP]-N^2-dG adducts.

Torsion Angles and Cyclization Efficiency. Cyclization efficiencies are strongly affected not only by bending at the sites of the lesions but also by the phasing of the two ends, which is a function of the overall twist of one end with respect to the other (*46*). The known twist angles for each pair of bases (*53*) yields a helical repeat of 10.49 ± 0.07 for the 11-mer sequence **I**. Thus, for a 99 base-pair circular molecule, the substrate for the T4 ligase, the twist of the two ends should be 157° out of phase, if changes in the twist at the lesion site are neglected. Shore et al. (*46*) have shown that, in the case of unmodified DNA, there is a precipitous drop in the cyclization efficiency when the twist angles at the two ends are that much out of phase. In the case of the (+)-*trans*-oligonucleotides **I** there appears to be a significant flexibility in the twist angles at the sites of the lesions that diminishes the unfavorable phasing effect associated with the intrinsic overall twist. For the 99 base pair circular molecule, the two ends of the molecule would be completely in phase if there were an untwisting of 157°, or 17° per 11-mer or [BP]-N^2-dG residue. While the untwisting associated with (+)-*trans*-[BP]-N^2-dG lesions in sequence **I** is not known, in supercoiled ϕX 174 DNA treated with (+)-*anti*-BPDE, the unwinding angle, averaged over all types of BP adducts and base sequence contexts, is 11.5 ± 4° per covalently bound BPDE residue (*27*). Therefore, the excess twist predicted from the base sequence **I** is at least partially compensated by an untwisting associated with the covalent *trans*-[BP]-N^2-dG residues. The highly efficient cyclization suggests that there is sufficient dynamic motion at the two ends of the molecules to bring the overall torsion angles in phase so as to allow the cohesive ends to form hydrogen bonds. The ligase then seals the two ends to produce a covalently closed circular DNA molecule.

The increased torsional and bending flexibility inferred from the highly efficient circularization of (+)-*trans*-[BP]-modified oligonucleotides seems analogous to the increased torsional flexibilities associated with DNA sequences containing three unpaired, noncomplementary purine-purine and pyrimidine-pyrimidine base pairs (*54*). The torsional flexibility associated with these DNA loops removes the requirement of the accurate alignment of the helical phased DNA ends, which depends on the number of helical turns (*46*) and causes a dramatic increase in the cyclization probability (*54*). Mills et al. (*55*) found that single-stranded gaps two to four nucleotides long positioned within normal double-stranded DNA sequences also dramatically increase the flexibility of DNA. These two examples suggest that the lack of proper hydrogen bonding (*54*) or the presence of single-stranded segments (*55*) greatly increases the flexibility of DNA. Similarly, the (+)-*trans*-*anti*-[BP]-N^2-dG lesions may locally increase the flexibility by destabilizing Watson−Crick base

pairing. Indeed, the thermodynamic stabilities of 11-mer duplexes (melting points T_m) with the same sequence context as **I** and with *trans-anti*-[BP]-N^2-dG lesions are reduced by up to 13° (*43*).

Conformational Heterogeneity, Flexibility, and the Effect of Local Sequence Context. The apparent flexibility associated with the (+)-*trans*-[BP]-N^2-dG lesions in the sequence context ...TG*T... in sequence **I** raises the possibility that multiple conformations might be observable in the NMR characteristics of this sequence. We therefore investigated the 1D and 2D NMR characteristics in the sequence context **I** with a fully complementary strand opposite the 11-mer modified strand and with G* = (+)-*trans*-[BP]-N^2-dG lesion (for details, see the Supporting Information). The imino proton spectrum clearly indicates that more than one conformer is present on the NMR time scale. The imino proton resonances in the central 5′-d(- - -ATG*- -)·d(- - -CAT- -) segment containing the lesion could not be assigned, thus preventing a full structural analysis of the modified duplex. Furthermore, the NOE connectivities from the base protons to their own and 5′-flanking sugar H1′ protons could be traced throughout the 11-mer duplex except within the central 5′-d(- - -ATG*- -)·d(- - -CAT- -) segment. The loss of the imino proton resonance signals in this region may be due to broadening effects associated with rapid base pair opening rates (*56*); theoretical considerations suggest that DNA bending and base pair separation are coupled to one another (*57*). Taken together, these observations are consistent with a relatively intact duplex at all base pairs except within the 5′-d(- - -ATG*- -)·d(- - -CAT- -) segment, which is correlated with the existence of multiple conformers that may interconvert slowly on the NMR time scale in sequence context **I**. In contrast, in the sequence

5'-C1--C2---A3--T4---C5---G6*--C7---T8---A9-C10--C11
G22-G21-T20-A19-G18-C17---G16-A15-T14-G13-G12 (II)

with G6* = (+)-*trans*-[BP]-N^2-dG, a single distinguishable conformation was observed with all 11 imino protons accounted for, and the NOE connectivities were traceable from one end of the duplex to the other, indicating further that all 11 base pairs were in the Watson−Crick conformation (*11*). The BP residues are positioned in the minor groove pointing toward the 5′-direction of the modified strand. In a related sequence with the same lesion positioned in the d(- - -T-G*-C- - -) sequence context, Fountain and Krugh (*13*) found a similar, minor groove adduct conformation; however, a second, less abundant conformer, in a slowly exchanging equilibrium with the minor groove conformation, was also observed.

The flexibility associated with sequence **I**, and to a lesser extent with the 5′-d(- - -TGC- - -)·d(- - -GCA- - -) sequence of Fountain and Krugh (*13*), is correlated with the presence of dT residues flanking the [BP]-modified G* residues on one or both sides. The thermodynamic stabilities of the hydrogen-bonded dA·dT base pairs are lower than those of dG·dC base pairs (*58*, *59*). This difference in thermodynamic stabilities may account for the flexibility associated with the (+)-*trans*-[BP]-N^2-dG lesions in duplex **I**, and the relatively rigid bends observed when guanines flank the (+)-*trans*-[BP]-N^2-dG lesions on both sides.[2] The sequence-dependent flexibility suggests an explanation for the observation, by NMR methods, of a single *trans*-[BP]-N^2-dG adduct conformation in the more rigid sequence **II**, and more than one conformer in the more flexible sequence contexts 5′-d(- - -TG*C- - -)·d(- - -GCA- - -) and 5′- -d(- - -TG*T- - -)·d(- - -ACA- - -).

The existence of more than one conformer in duplexes containing other bulky carcinogen-DNA adducts has been observed as well. Examples include *N*-acetyl-2-aminofluorene (AAF) covalently bound to C8-dG in the sequence context CG*C (*60*) and N-2-aminofluorene (AF) bound covalently to C8-dG in the TG*A and AG*G sequence context within the codon 61 of the mouse (*61*) and human c-Ha-*ras* 1 protooncogene (*62*, *63*).

Biological Implications. The relationships between adduct conformation and mutagenic specificity is a subject of great current interest (*64*). The hypothesis that one and the same carcinogen−DNA adduct can assume multiple conformations in different or even the same base sequence context, and thus engender different patterns of mutation, has been discussed by a number of researchers (*13*, *62*, *63*, *65*, *66*). Our results, in conjunction with previous NMR conformational studies (*11*, *13*), suggest that a sequence-dependent flexibility at the [BP]-N^2-dG lesion sites gives rise to a more heterogeneous distribution of adduct conformations. Analogous sequence-dependent effects may allow for adduct structural heterogeneities at DNA replication forks, thus leading to base sequence-dependent mutation spectra. Systematic studies of the effects of base sequence on mutation frequencies and mutagenic specificities in site-directed mutagenesis experiments seem particularly timely in view of the emerging data on sequence effects on adduct conformations (*10*) and adduct-induced bending.[2]

The binding of proteins to DNA induces bending, which is important in DNA packaging and which may play a role in the regulation of transcription, replication, and recombination [see, for example, *67*−*69*]. The binding to DNA of Cro (*70*) or CAP protein (*71*) induces DNA bending and greatly enhances the cyclization efficiency upon ligation. Furthermore, the CAP protein binds ∼200 times more effectively to circularized than to linear DNA, thus showing that this protein binds much more strongly to bent rather than to linear DNA recognition sequences. Thus, bending associated with the covalent binding of *anti*-BPDE to DNA may significantly affect the binding affinities of the modified sequences with critically important cellular proteins. Base sequence effects of BPDE−DNA adducts on bending and flexibility may lead to local distortions in the DNA conformation that may also have profound effects on the rates of nucleotide excision repair. Zou et al. (*15*) have shown that the rates of excision by UvrABC proteins of *anti*-[BP]-N^2-dG lesions in sequence context **II** are remarkably dependent on the stereochemical properties of the lesions; however, the effects of base sequence on damage recognition and excision have not yet been investigated.

In summary, the extraordinary differences in the bending and circularization efficiencies and flexibilities associated with the (+)-*trans*- and (−)-*trans*-[BP]-N^2-dG lesions in duplex **I** indicate that the tumorigenic (+)-*anti*-BPDE and the nontumorigenic enantiomer (−)-*anti*-BPDE give rise to very different kinds of deformations upon binding covalently to DNA. The detailed bases of these structure-activity relationships remain to be elucidated.

ACKNOWLEDGMENT

We wish to thank Professors W. Olson, A. Vologodskii, and E. Trifonov for stimulating discussions.

SUPPORTING INFORMATION AVAILABLE

Two figures showing 1-D and 2-D NMR data for the duplex 5′-d(CACAT[G*]TACAC)·d(GTGTACATGTG) with G* = (+)-*trans*-*anti*-[BP]-N^2-dG (5 pages). Ordering information is given on any current masthead page.

REFERENCES

1. Conney, A. H. (1982) *Cancer Res. 42*, 4875−4917.
2. Buening, M. K., Wislocki, P. G., Levin, W., Yagi, H., Thakker, D. R., Akagi, H., Koreeda, M., Jerina, D. M., and Conney, A. H. (1978) *Proc. Natl. Acad. Sci. U.S.A. 75*, 5358−5361.
3. Slaga, T. J., Bracken, W. J., Gleason, G., Levin, W., Yagi, H., Jerina, D. M., and Conney, A. H. (1979) *Cancer Res. 39*, 67−71.
4. Wood, A. W., Chang, R. L., Levin, W., Yagi, H., Thakker, D. R., Jerina, D. M., and Conney, A. H. (1977) *Biochem. Biophys. Res. Commun. 77*, 1389−1396.
5. Brookes, P., and Osborne, M. R. (1982) *Carcinogenesis 3*, 1223−1226.
6. Stevens, C. W., Bouck, N., Burgess, J. A., and Fahl, W. E. (1985) *Mutat. Res. 152*, 5−14.
7. Wei, S.-J. C., Chang, R. L., Hennig, E., Cui, X. X., Merkler, K. A., Wong, C.-Q., Yagi, H., and Conney, A. H. (1994) *Carcinogenesis 15*, 1729−1735.
8. Meehan, T., and Straub, K. (1979) *Nature 277*, 410−412.
9. Cheng, S. C., Hilton, B. D., Roman, J. M., and Dipple, A. (1989) *Chem. Res. Toxicol. 2*, 334−40.
10. Geacintov, N. E., Cosman, M., Hingerty, B. E., Amin, S., Broyde, S., and Patel, D. J. (1997) *Chem. Res. Toxicol. 10*, 111−146.
11. Cosman, M., de los Santos, C., Fiala, R., Hingerty, B. E., Ibanez, V., Margulis, L. A., Live, D., Geacintov, N. E., Broyde, S., and Patel, D. J. (1992) *Proc. Natl. Acad. Sci. U.S.A. 89*, 1914−1918.
12. de los Santos, Cosman, M., Hingerty, B. E., Ibanez, V., Margulis, L. A., Geacintov, N. E., Broyde, S., and Patel, D. J. (1992) *Biochemistry 31*, 5245−5252.
13. Fountain, M. A., and Krugh, T. R. (1995) *Biochemistry 34*, 3152−3161.
14. Mao, B., Li, B., Amin, S., Cosman, M., and Geacintov, N. E. (1993) *Biochemistry 32*, 11785−11793.
15. Zou, Y., Liu, T., Geacintov, N. E., and Van Houten, B. (1995) *Biochemistry 34*, 13582−13593.
16. Choi, D.-J., Marino-Alessandri, D. J., Geacintov, N. E., and Scicchitano, D. A. (1994) *Biochemistry 33*, 780−787.
17. Hruszkewycz, A. M., Canella, K. A., Peltonen, K., Kotrappa, L., and Dipple, A. (1992) *Carcinogenesis* 13, 2347−2352.
18. Shibutani, S., Margulis, L. A., Geacintov, N. E., and Grollman, A. P. (1993) *Biochemistry 32*, 7531−7541.
19. Mackay, W., Benasutti, M., Drouin, E., and Loechler, E. L. (1992) *Carcinogenesis 13*, 1415−1425.
20. Jelinsky, S. A., Liu, T., Geacintov, N. E., and Loechler, E. L. (1995) *Biochemistry 34*, 13545−13553.
21. Moriya, M., Spiegel, S., Fernandes, A., Amin, S., Liu, T., Geacintov, N., and Grollman, A. P. (1996) *Biochemistry 35*, 16646−16651.
22. Schwartz, A., Marrot, L., and Leng, M. (1989) *J. Mol. Biol. 207*, 445−50.
23. Leng, M. (1990) *Biophys. Chem. 35*, 155−163.
24. Hogan, M. E., Dattagupta, N., and Whitlock, J. P., Jr. (1981) *J. Biol. Chem. 256*, 4504−4513.
25. Eriksson, M., Nordén, B., Jernström, B., and Gräslund, A. (1988) *Biochemistry 27*, 1213−1221.
26. Roche, C. J., Geacintov, N. E., Ibanez, V., and Harvey, R. G. (1989) *Biophys. Chem. 33*, 277−288.
27. Xu, R., Birke, S., Carberry, S. E., Geacintov, N. E., Swenberg, C. E., and Harvey, R. G. (1992) *Nucl. Acids Res. 20*, 6167−6176.
28. Xu, R., Mao, B., Xu, J., Li, B., Birke, S., Swenberg, C. E., and Geacintov, N. E. (1995) *Nucl. Acids Res. 23*, 2314−9.
29. Suh, M., Ariese, F., Small, G. J., Jankowiak, R., Liu, T.-M., and Geacintov, N. E. (1995) *Biophys. Chem. 56*, 281−296.
30. Liu, T., Xu, J., Tsao, H., Li, B., Xu, R., Yang, C., Moriya, M., and Geacintov, N. E. (1996). *Chem. Res. Toxicol. 9*, 255−261.
31. Marini, J. C., Levene, S. D., Crothers, D. M., and Englund, P. T. (1982) *Proc. Natl. Acad. Sci. U.S.A. 79*, 7664−7668.
32. Trifonov, E. N. (1985) *CRC Crit. Rev. Biochem. 19*, 89−106.
33. Diekmann, S. (1992) *Methods Enzymol. 212*, 30−46.
34. Seela, F., Berg, H., and Rosemeyer, H. (1989) *Biochemistry 28*, 6193−6198.
35. Bellon, S. F., and Lippard, S. J. (1990) *Biophys. Chem. 35*, 179−88.
36. Lee, C.-S., Sun, D., Kizu, R., and Hurley, L. H. (1991) *Chem. Res. Toxicol. 4*, 203−213.
37. Shore, D., Langowski, J., and Baldwin, R. L. (1981) *Proc. Natl. Acad. Sci. U.S.A. 78*, 4833−4837.
38. Ulanovsky, L., Bodner, M., Trifonov, E. N., and Choder, M. (1986) *Proc. Natl. Acad. Sci. U.S.A. 83*, 862−6.
39. Koo, H.-S., and Crothers, D. M. (1988) *Proc. Natl. Acad. Sci. U.S.A. 85*, 1763−1767.
40. Lyubchenko, Y. L., Shlyakhtenko, L. S., Appella, E., and Harrington, R. E. (1993) *Biochemistry 32*, 4121−7.
41. McLaughlin, L. W., and Piel, N. (1984) In *Oligonucleotide Synthesis: A Practical Approach* (Gait, M. J., Ed.), pp 117−133, IRL Press, Oxford.
42. Geacintov, N. E., Cosman, M., Mao, B., Alfano, A., Ibanez, V., and Harvey, R. G. (1991) *Carcinogenesis 12*, 2099−2108.
43. Cosman, M., Geacintov, N. E., and Amin, S. (1993) *Polycyclic Aromatic Compounds. Synthesis, Properties, Analytical Measurements, Occurrence and Biological Effects* (Garrigues, P., and Lamotte, M., Eds.), pp 1151−1158, Gordon & Breach, Switzerland.
44. Zahn, K., and Blattner, F. R. (1987) *Science 236*, 416−22.
45. Livshits, M. A., and Lyubchenko, Y. L. (1994) *Molekul. Biologiya 28*, 1069−1077 (English Trans.: *28*, 687−690).
46. Shore, D., and Baldwin, R. L. (1983) *J. Mol. Biol. 170*, 957−981.
47. Jacobson, H., and Stockmayer, W. H. (1950) *J. Chem. Phys. 18*, 1600−1606.
48. Gobush, W., Yamakawa, H., Stockmayer, W. H., and Magee, W. S. (1972) *J. Chem. Phys. 57*, 2839−43.
49. Crothers, D. M., Drak, J., Kahn, J. D., and Levene, S. D. (1992) *Methods Enzymol. 212*, 3−29.
50. Husain, I., Griffith, J., and Sancar, A. (1988) *Proc. Natl. Acad. Sci. U.S.A. 85*, 2558−2562.
51. Hagerman, P. J. (1988) *Annu. Rev. Biophys. Biophys. Chem. 17*, 265−286.
52. Bolshoy, A., McNamara, P., Harrington, R. E., and Trifonov, E. N. (1991) *Proc. Natl. Acad. Sci. U.S.A. 88*, 2312−2316.
53. Kabsch, W., Sander, C., and Trifonov, E. N. (1982) *Nucl. Acids Res. 10*, 1097−1104.
54. Khan, J. D., Yun, E., and Crothers, D. M. (1994) *Nature 368*, 163−166.
55. Mills, J. B., Cooper, J. M., and Hagerman, P. J. (1994) *Biochemistry 33*, 1797−1803.
56. Kochoyan, M., Leroy, J. L., and Guéron, M. (1987) *J. Mol. Biol. 196*, 599−609.
57. Ramstein, J., and Lavery, R. (1988) *Proc. Natl. Acad. Sci. U.S.A. 85*, 7231−7235.
58. Breslauer, K. J., Frank, R., Blöcker, H., and Marky, L. A. (1986) *Proc. Natl. Acad. Sci. U.S.A. 83*, 3746−3750.
59. SantaLucia, J., Jr., Allawi, H. T., and Seneviratne, P. A. (1996) *Biochemistry 35*, 3555−3562
60. O'Handley, S. F., Sanford, D. G., Xu, R., Lester, C. C., Hingerty, B. E., Broyde, S., and Krugh, T. R. (1993) *Biochemistry 32*, 2481−2497.
61. Cho, B. P., Beland, F. A., and Marques, M. M. (1994) *Biochemistry 33*, 1373−1384.

62. Eckel, L. M., and Krugh, T. R. (1994) *Nature Struct. Biol. 1*, 89−94.
63. Eckel, L. M., and Krugh, T. R. (1994) *Biochemistry 33*, 13611−13624.
64. Loechler, E. L. (1995) *Mol. Carcinogenesis 13*, 213−219.
65. Veaute, X., and Fuchs, R. P. P. (1991) *Nucleic Acids Res. 19*, 5603−5606.
66. Rodriguez, H., and Loechler, E. L. (1995) *Mutat. Res. 326*, 29−37.
67. Travers, A. A. (1990) *Cell 60*, 177−180.
68. Crothers, D. M., Gartenberg, M. R., and Shrader, T. E. (1991) *Meth. Enzymol. 208*, 118−146.
69. Kerppola, T. K., Curran, T. (1991) *Science 254*, 1210−1214.
70. Lyubchenko, L., Shlyakhtenko, L., Chernov, B., and Harrington, R. E. (1991) *Proc. Natl. Acad. Sci. U.S.A. 88*, 5331−5334.
71. Kahn, J. D., and Crothers, D. M. (1992) *Proc. Natl. Acad. Sci. U.S.A. 89*, 6343−6347.

BI971785X